

Enhanced mechanical properties of nanostructured TiSi₂-NbSi₂ composite rapidly sintered by pulsed current activated heating

Bong-Won Kwak^a, Byung-Su Kim^b, Jin-Kook Yoon^c, Kyung-Tae Hong^c and In-Jin Shon^{a,*}

^aDivision of Advanced Materials Engineering and the Research Center of Advanced Materials Development, Engineering College, Chonbuk National University, Chonbuk 561-756, Korea

^bMinerals Resources Research Division, Korea Institute of Geoscience and Mineral Resources, Daejeon, 305-350, Korea

^cMaterials Architecturing Research Center, Korea Institute of Science and Technology, PO Box 131, Cheongryang, Seoul 130-650, Korea

Despite of many attractive properties, the low fracture toughness of refractory metal silicides limits their wide application. One of the most obvious tactics to improve the mechanical properties has been to make fabrication of a nanostructured material and composite material. Nanopowders of Ti, Nb, and Si were fabricated by high-energy ball milling. A dense nanostructured TiSi₂-NbSi₂ composite was simultaneously synthesized and sintered by the pulsed current activated sintering method within three minutes using mechanically activated powders of Ti, Nb, and Si. A high-density TiSi₂-NbSi₂ composite was produced under simultaneous application of an 80-MPa pressure and a pulsed current. The hardness and fracture toughness of the nanostructured TiSi₂-NbSi₂ composite were higher than those of monolithic TiSi₂ or NbSi₂. This is believed to suggest that TiSi₂ and NbSi₂ in the composite may deter the propagation of cracks and TiSi₂ and NbSi₂ have a nanocrystalline.

Key words: Composites, Nanostructures, Sintering, Synthesis, Mechanical properties.

Introduction

Interest in refractory metal silicides has increased significantly in recent years because of their potential application as high-temperature structural materials [1]. This class of materials has an attractive combination of properties, including high melting temperature, high modulus, high oxidation resistance in air, and a relatively low density [2, 3]. Furthermore, the disilicides, in particular TiSi₂, and NbSi₂, have been used as Schottky barriers, ohmic contacts, gate materials, and interconnectors in integrated circuits, as a result of their low electrical resistivity, high stability, and good compatibility with silicon substrates [4,5]. However, as in the case of many similar compounds, the current concern about these materials (TiSi₂ and NbSi₂) focuses on their low fracture toughness below the ductile-brittle transition temperature [6, 7]. To improve the mechanical properties of these materials, the fabrication of a nanostructured material and composite material [8-11] have been found to be effective.

Recently, nanocrystalline powders have been produced by high-energy milling [12, 13]. The sintering temperature of high-energy mechanically milled powder is lower than that of unmilled powder due to the increased reactivity, internal and surface energies, and

surface area of the milled powder, which contribute to its so-called mechanical activation [14-16]. The grain size in sintered materials becomes much larger than that in pre-sintered powders due to rapid grain growth during a conventional sintering process. Therefore, controlling grain growth during sintering is one of the keys to the commercial success of nanostructured materials. In this regard, the pulsed current activated sintering method (PCASM), which can make dense materials within 2 minutes, has been shown to be effective in achieving not only rapid densification to near theoretical density, but also the prohibition of grain growth in nanostructured materials [17-19].

This paper reports on the rapid synthesis and consolidation of dense nanostructured TiSi₂-NbSi₂ composite starting with high-energy ball-milled nanopowders. The mechanical properties and grain sizes of the resulting nanostructured TiSi₂-NbSi₂ composite were also evaluated.

Experimental Procedures

Powders of 99.9% pure titanium (-325 mesh, Alfa Products), 99.5% pure silicon (-325 mesh, Aldrich Products), and 99.8% pure niobium (-325 mesh, Alfa Products) were used as starting materials. 0.5Ti, 0.5Nb, and 2Si powder mixtures were first milled in a high-energy ball mill (Pulverisette-5 planetary mill) at 250 rpm and for 10 h. Tungsten carbide balls (9 mm in diameter) were used in a sealed cylindrical stainless steel vial under an argon atmosphere. A charge ratio (ratio of ball mass to powder) of 30 : 1 was used. The

*Corresponding author:
Tel : +82-63-270-2381
Fax : +82-63-270-2386
E-mail: ijshon@chonbuk.ac.kr

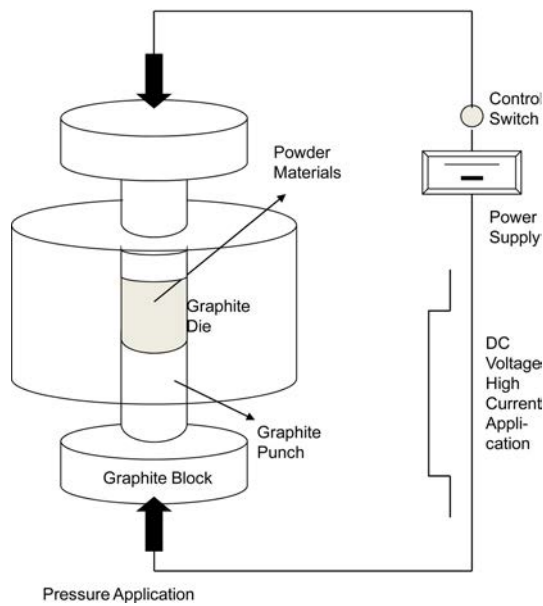


Fig. 1. Schematic diagram of the pulsed current activated sintering apparatus.

grain size was calculated using Suryanarayana and Grant Norton's formula [20]:

$$B_r (B_{\text{crystalline}} + B_{\text{strain}}) \cos\theta = k \lambda / L + \eta \sin\theta \quad (1)$$

where B_r is the full width at half-maximum (FWHM) of the diffraction peak after an instrumental correction; $B_{\text{crystalline}}$ and B_{strain} are the FWHM caused by the grain size and internal stress, respectively; k is a constant (with a value of 0.9); λ is the wavelength of the X-ray radiation; L and η are the grain size and internal strain, respectively; and θ is the Bragg angle. The parameters, B and B_r , follow the Cauchy's form with the relationship $B = B_r + B_s$, where B and B_s are the FWHM of the broadened Bragg peaks and the standard Bragg peaks of the samples, respectively.

After milling, the powder was placed in a graphite die (outside diameter = 35 mm, inside diameter = 10 mm, and height = 40 mm), and then introduced into the pulsed current activated sintering system, shown schematically in Fig. 1. The four major stages in the synthesis are as follows: evacuation of the system to 40 mtorr (stage 1), application of a uniaxial pressure of 80 MPa (stage 2), activation of a pulsed current (on time; 20 μ s, off time; 10 μ s), which was maintained until densification was attained as indicated by a linear gauge measuring the shrinkage of the sample (stage 3), and cooling the sample to room temperature (stage 4). Temperatures were measured by a pyrometer focused on the surface of the graphite die. The process was carried out under a vacuum of 40 mtorr (5.3 Pa).

The relative densities of the sintered samples were measured by the Archimedes method. Microstructural information was obtained from product samples, which were polished and etched for 1 minute at room

temperature using a solution composed of HF (10 vol.%), HNO_3 (30 vol.%), and H_2O (60 vol.%). Compositional and microstructural analyses of the products were made through X-ray diffraction (XRD) and scanning electron microscopy (SEM) with energy dispersive X-ray analysis (EDAX). Vickers hardness was measured by performing indentations with a load of 1 kg and a dwell time of 15 s on the synthesized samples.

Results and Discussion

Fig. 2 shows SEM images of the raw powders used. All powders have angular shapes. XRD patterns of raw powders and milled 0.5Ti-0.5Nb-2Si powders are shown in Fig. 3. In Fig. 3(d), only Ti, Nb, and Si peaks were observed, as marked. Therefore, it is obvious that no chemical reaction occurred between the component powders during milling. Nevertheless, the peaks of the powders are significantly wide, suggesting that their grain sizes became very fine due to the milling. Fig. 4

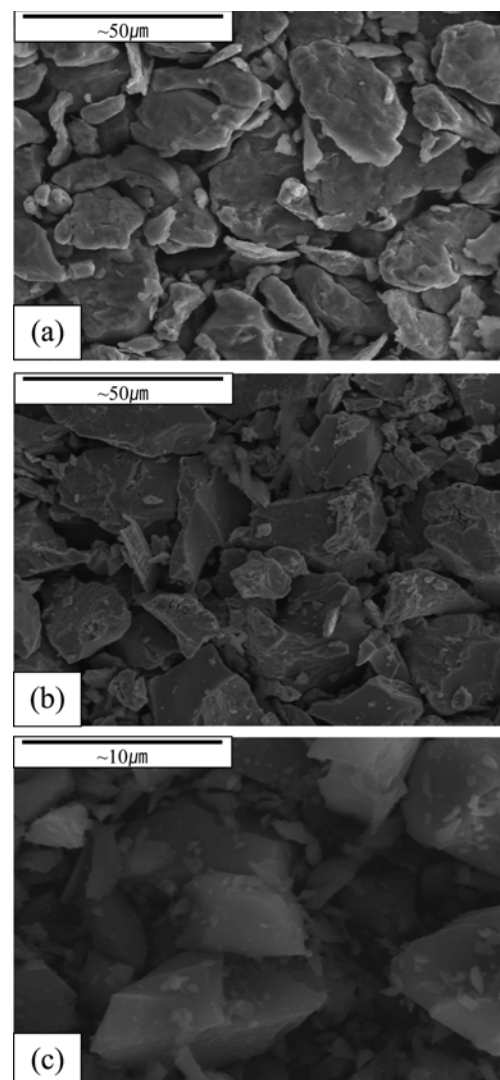


Fig. 2. SEM images of raw materials: (a) Ti, (b) Nb, and (c) Si.

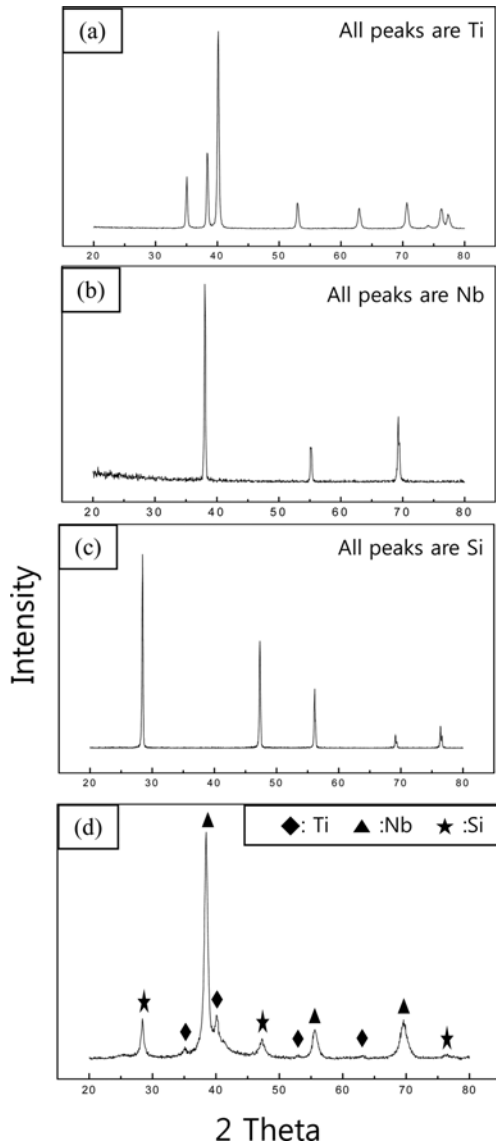


Fig. 3. XRD patterns of raw materials: (a) Ti, (b) Nb, (c) Si, and (d) milled 0.5Ti-0.5Nb-2Si powder.

shows $\sin\theta$ versus $Br \cos\theta$ to calculate grain sizes of Nb, Ti and Si using Suryanarayana and Grant Norton's formula [20]. The average grain size of Ti, Nb, and Si was about 67, 282, and 19 nm, respectively. Fig. 5 shows a SEM image and X-ray mapping of milled powders. The milled powders have a very fine grain size and some agglomeration. In X-ray mapping, Si, Nb and Ti element were homogeneously distributed.

The shrinkage displacement-time (temperature) curve provides a useful information on the consolidation behavior. The variations in shrinkage displacement and temperature of the surface of the graphite die upon heating during the synthesis and densification of 0.5TiSi₂-0.5NbSi₂ composite are shown in Fig. 6. As the pulsed current was applied, the shrinkage displacement is nearly constant with temperature, and then abruptly increased. Fig. 7 shows the X-ray diffraction result of the sample heated to 1050 °C. The reactant peaks of Ti,

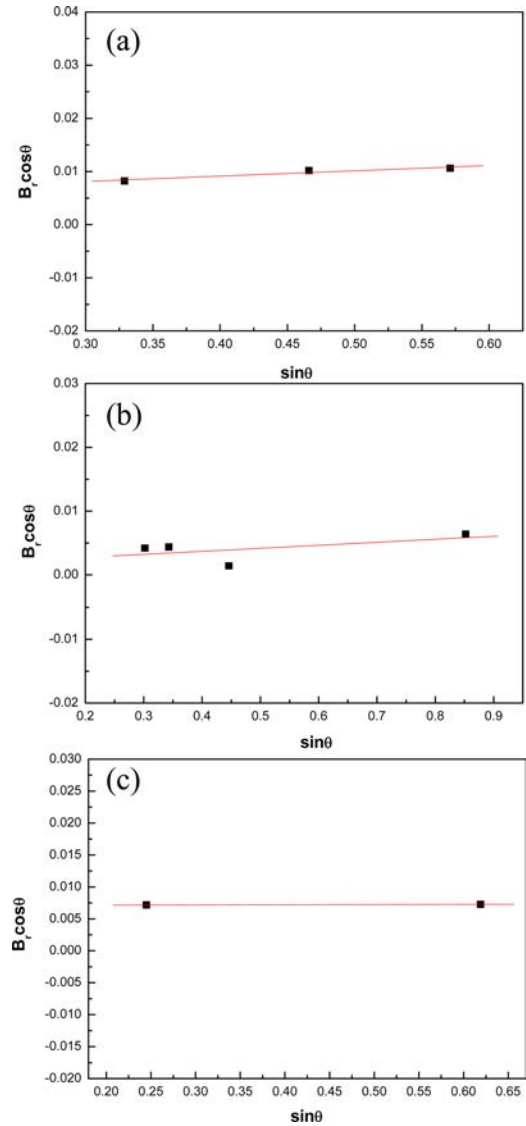


Fig. 4. Plot of $Br \cos\theta$ versus $\sin\theta$ of Nb(a), Ti(b) and Si(c) powders milled 10 h.

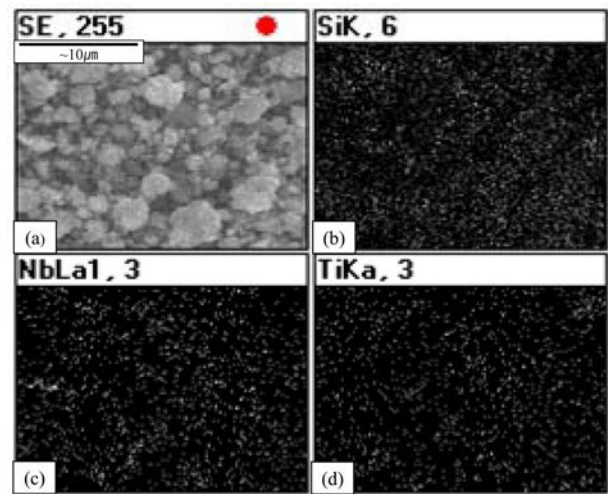


Fig. 5. SEM image and X-ray mapping of the milled 0.5Ti-0.5Nb-2Si powder: (a) SEM image, (b) silicon mapping, (c) niobium mapping, and (d) titanium mapping.

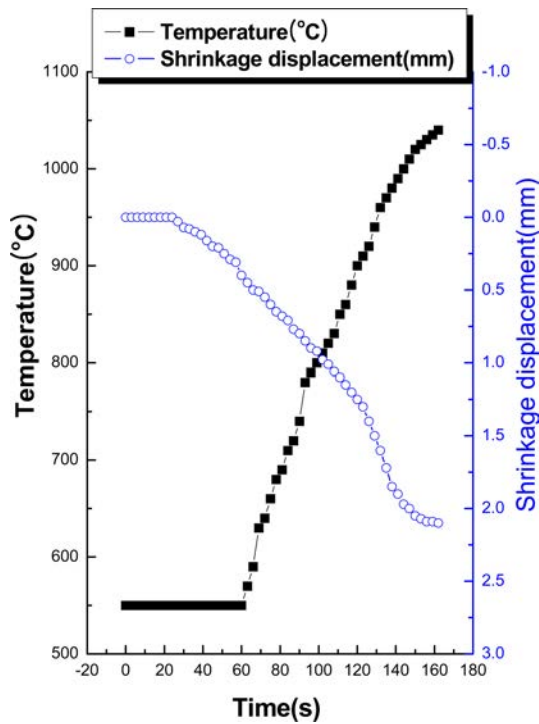


Fig. 6. Variations of temperature and shrinkage displacement with heating time during synthesis and densification of the $0.5TiSi_2-0.5NbSi_2$ composite.

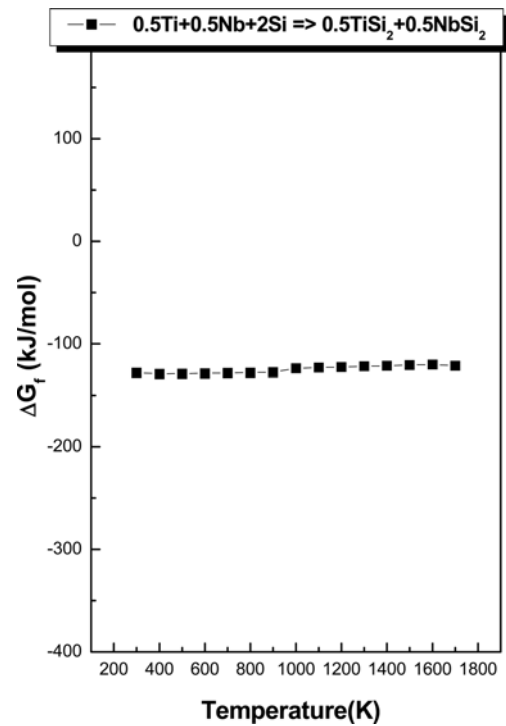


Fig. 8. Temperature dependence of the Gibbs free energy change by interaction of the $0.5Ti + 0.5Nb + 2Si$.

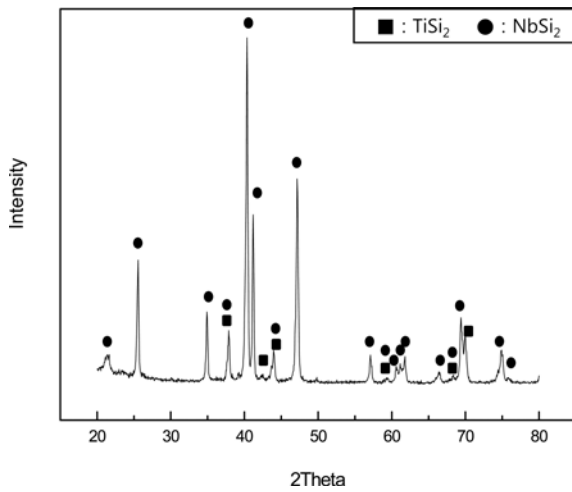
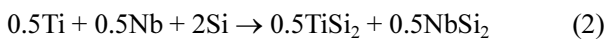


Fig. 7. XRD patterns of the $0.5Ti-0.5Nb-2Si$ system heated at $1050\text{ }^\circ\text{C}$.

Nb, and Si were not detected and product peaks of $TiSi_2$ and $NbSi_2$ were observed. The abrupt increase in the shrinkage displacement at the ignition temperature is due to the increase in density resulting from the change in the molar volume associated with the formation of $TiSi_2$ and $NbSi_2$ from the reactants (Ti, Nb, and Si) and the consolidation of the product. The interaction between these phases, i.e.,



is thermodynamically feasible, as shown in Fig. 8.

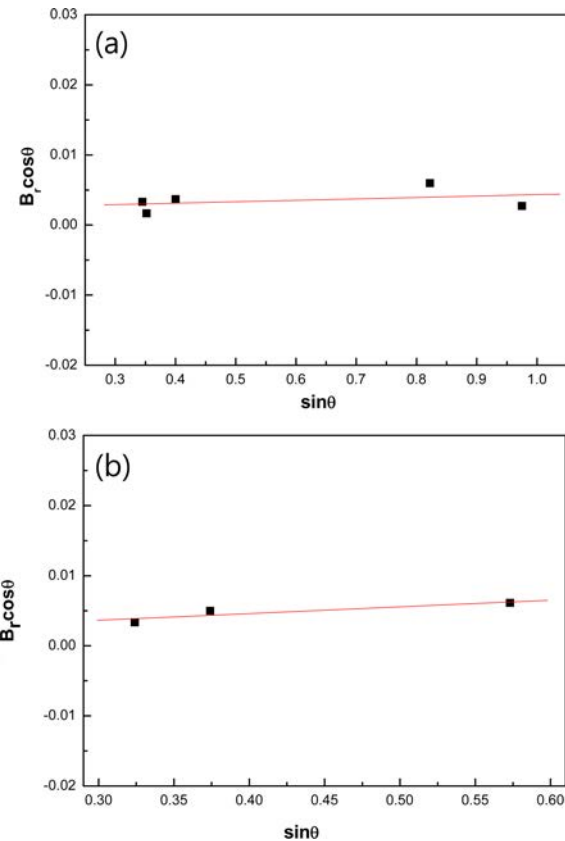


Fig. 9. Plot of $B_r \cos\theta$ versus $\sin\theta$ of $NbSi_2$ (a) and $TiSi_2$ (b) in composite.

Fig. 9 shows $\sin\theta$ versus $B_r \cos\theta$ to calculate grain sizes of $TiSi_2$ and $NbSi_2$ using Suryanarayana and Grant

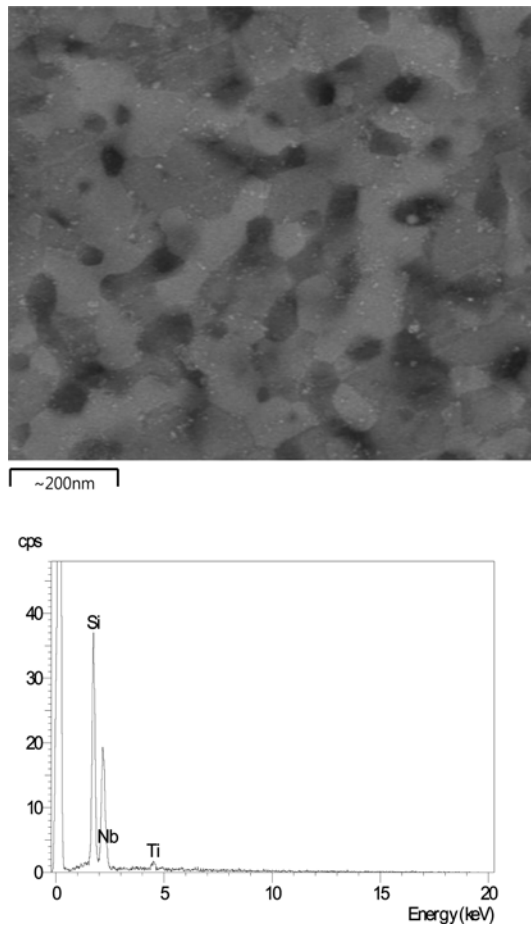


Fig. 10. FE-SEM image and EDS of $0.5\text{TiSi}_2\text{-}0.5\text{NbSi}_2$ composite sintered at $1050\text{ }^\circ\text{C}$.

Norton's formula [20] The average grain size of TiSi_2 and NbSi_2 was about 164 and 81 nm, respectively. A FE-SEM image and EDS of the etched surface of the sample heated to $1050\text{ }^\circ\text{C}$ under a pressure of 80 MPa is shown in Fig. 10. The microstructure consists of nanophases in the FE-SEM image. The corresponding relative density is 100%. In EDS, only Ti, Nb, and Si peaks were detected. The milling process is known to introduce impurities from the ball and/or container. However, in this study, peaks of Fe and W was not identified.

The role of the current during sintering and/or synthesis has been the focus of several attempts to provide an explanation for the observed sintering enhancement and the improved product characteristics. The role played by the current has been broadly interpreted by several groups. The effect has been explained by rapid heating due to Joule heating at contacts points, the presence of plasma in pores separating powder particles, and the intrinsic contribution of the current to mass transport [21-24].

Vickers hardness measurements were made on polished sections of the $0.5\text{TiSi}_2\text{-}0.5\text{NbSi}_2$ composite using a 1-kg load and 15-s dwell time. The calculated

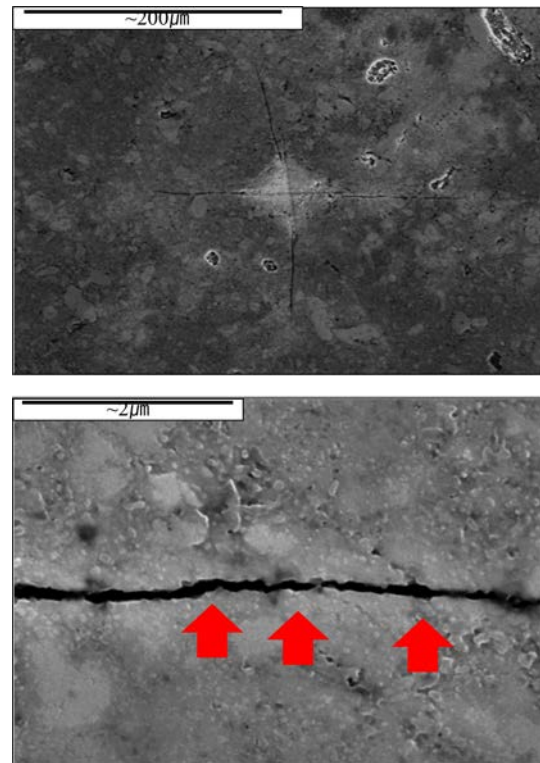


Fig. 11. (a) Vickers hardness indentation and (b) median crack propagation in the $0.5\text{TiSi}_2\text{-}0.5\text{NbSi}_2$ composite.

hardness value of the $0.5\text{TiSi}_2\text{-}0.5\text{NbSi}_2$ composite was 1105 kg/mm^2 . This value represents an average of five measurements. Indentations with large enough loads produced median cracks around the indentations. The length of these cracks permits an estimation of the fracture toughness for the material. From the length of these cracks, fracture toughness values can be determined using the formula developed by Anstis *et al.* [25], which is

$$K_{IC} = 0.016 (E/H)^{1/2} \cdot P/C^{3/2} \quad (3)$$

where E is Young's modulus, H is the indentation hardness, P is the indentation load, and C is the trace length of the crack measured from the center of the indentation. The modulus was estimated by the rule of mixtures for the 0.474 volume fraction of TiSi_2 and the 0.526 volume fraction of NbSi_2 using $E(\text{TiSi}_2) = 250\text{ GPa}$ [26] and $E(\text{NbSi}_2) = 362.8\text{ GPa}$ [27]. As in the case of hardness values, the toughness values were derived from the average of five measurements. The toughness value obtained by this method of calculation is $3.8\text{ MPa} \cdot \text{m}^{1/2}$.

Fig. 11 shows Vickers indentations in the $0.5\text{TiSi}_2\text{-}0.5\text{NbSi}_2$ composite sintered from milled powders. One to three additional cracks were observed to propagate from the indentation corners. These fracture toughness and hardness values of the nanostructured $0.5\text{WSi}_2\text{-}0.5\text{TaSi}_2$ composite are higher than those (fracture toughness; $2.9\text{ MPa} \cdot \text{m}^{1/2}$ hardness; 964 kg/mm^2) of the microstructured TiSi_2 [6] or

those (fracture toughness; 3.0 MPa · m^{1/2} hardness; 906 kg/mm²) of the nanostructured NbSi₂ [7]. A higher magnification view of the indentation median crack in the composite is shown in Fig. 11(b). This shows that the crack propagates in a deflective manner (↑). This is believed to suggest that TiSi₂ and NbSi₂ in the composite may deter the propagation of cracks.

Conclusions

Ti, Nb and Si nanopowders were fabricated using high-energy ball milling for 10 h. Using the pulsed current activated sintering method, a 0.5TiSi₂-0.5NbSi₂ composite was simultaneously synthesized and consolidated using the mechanically activated powders of 0.5Ti, 0.5Nb, and 2Si within three minutes. The relative density of the composite was 100% for the applied pressure of 80 MPa. The average grain sizes of TiSi₂ and NbSi₂ in 0.5TiSi₂-0.5NbSi₂ composite sintered by this method were determined as 164 and 81 nm, respectively. The average hardness and fracture toughness values obtained were 1105 kg/mm² and 3.8 MPa · m^{1/2}, respectively. These fracture toughness and hardness values of the nanostructured 0.5TiSi₂-0.5NbSi₂ composite are higher than those of monolithic TiSi₂ or NbSi₂. This is believed to suggest that TiSi₂ and NbSi₂ in the composite may deter the propagation of cracks and TiSi₂ and NbSi₂ have nanophases.

Acknowledgments

This work was supported by the KIST Institutional Program (Project No. 2E25374-15-096) and was supported by a grant in aid awarded by the Basic Research Project of the Korea Institute of Geoscience and Mineral Resources (KIGAM), funded by the Ministry of Science, ICT and Future Planning (GP2015036).

References

1. N.S. Stoloff, Mater. Sci. Eng. A 261, (1999) 169-180.
2. A.K. Vasudevan, J.J. Petrovic, Mater. Sci. Eng. A 155, (1992) 259-266.
3. G.J. Fan, M.X. Quan, Z.Q. Hu, J. Eckert, L. Schulz, Scripta Mater. 41, 1147-1151 (1999) 1147-1151.
4. M.E. Schlesinger, Chem Rev 90, (1990) 607-628.
5. A.K. Vasudevan, J.J. Petrovic, Mater Sci Eng. A 155, (1992) 1-17.
6. Byung-Ryang Kim, Kee-Seok Nam, Jin-Kook Yoon, Jung-Mann Doh and In-Jin Shon, Journal of Ceramic Processing Research. 10, (2008) 171-175.
7. Byung-Ryang Kim, Jin-Kook Yoon, Kee-Seok Nam, In-Jin Shon, Journal of Korean Powder Metallurgy Institute, 15, 279-284 (2010) 279-284.
8. In-Jin Shon, Hyoung-Gon Jo, and Hanjung Kwon, Korean J. Met. Mater., 52, (2014) 343-346.
9. Y. Ohya, M. J. Hoffmann, G. Petzow, J Am Ceram Soc. 75, (1992) 2479-2483.
10. S. K. Bhaumik, C. Divakar, A. K. Singh, G. S. Upadhyaya, J Mater Sci Eng. A 279, (2000) 275-281.
11. Geon-Woo Lee, In-Jin Shon, Korean J. Met. Mater., 51, 95-100 (2014) 95-100.
12. Seung-Mi Kwak, Hyun-Kuk Park, and In-Jin Shon, Korean J. Met. Mater. 51, (2013) 341-348.
13. Na-Ra Park, Kwon-Il Na, Han-jung Kwon, Jae-Won Lim, and In-Jin Shon, Korean J. Met. Mater. 51, (2013) 753-759.
14. F. Charlot, E. Gaffet, B. Zeghmati, F. Bernard, J. C. Liepce, Mater. Sci. Eng. A262, (1999) 279-287.
15. In-Jin Shon, Ik-Hyun Ohb, Jung-Han Ryu, Jun-Ho Jang, Hee-Jun Youn and Hyun-Kuk Park, Journal of Ceramic Processing Research. Vol. 14, No. 5, (2013) 641-647.
16. M.K. Beyer, H. Clausen-Schaumann, Chem. Rev. 105, (2005) 2921-2948.
17. Song-Lee Du, Jung-Mann Doh, Jin-Kook Yoon, and In-Jin Shon, Korean J. Met.Mater., 51, (2013) 579-584.
18. I.J. Shon, S.L. Du, J.M. Doh, J.K. Yoon, Met. Mater. Int. 19, (2013) 1041-1045.
19. In-Jin Shon, Korean J. Met. Mater., 52, (2014) 573-580.
20. C. Suryanarayana, M. Grant Norton, X-ray Diffraction A Practical Approach, Plenum Press, New York (1998).
21. Z. Shen, M. Johnsson, Z. Zhao and M. Nygren, J. Am. Ceram. Soc. 85, (2002) 1921-1927.
22. J. E. Garay, U. Anselmi-Tamburini, Z. A. Munir, S. C. Glade and P. Asoka- Kumar, Appl. Phys. Lett. 85, (2004) 573-575.
23. J. R. Friedman, J. E. Garay. U. Anselmi-Tamburini and Z. A. Munir, Intermetallics. 12, (2004) 589-597.
24. J. E. Garay, J. E. Garay. U. Anselmi-Tamburini and Z. A. Munir, Acta Mater., 51, (2003) 4487-4495.
25. G.R. Anstis, P. Chantikul, B.R. Lawn, D.B. Marshall, J. Am. Ceram. Soc. 64, (1981) 533-538.
26. Dalibor Vojtěch, Barbora Bártová, Tomáš Kubatík, Materials Science and Engineering A361 (2003) 50-57.
27. F. CHU, MING LEI, S. A. MALOY, J. J. PETROVIC and T. E. MITCHELL, Acta mater. Vol. 44, No. 8, (1996) 3035-3048.